1993 SCA Conference Paper Number 9313

Studies of Rock Structures Using NMR Restricted Diffusion Measurements and Analyses

Songhua Chen, Jinli Qiao, Hsie-Keng Liaw, and A. Ted Watson
Department of Chemical Engineering, Texas A&M University, College Station, TX 77843-3122

Abstract

Pulsed field gradient nuclear magnetic resonance techniques were used to study sandstone and limestone systems with different structural characteristics. Stimulated echo sequences with four bipolar gradient pulses were used in the measurements to reduce the effects of the internal field gradients arising from the structural and chemical composition heterogeneities. It is found that the rock permeability differences can be detected by analyzing the diffusion characteristics. In addition, a set of diffusion measurements was performed on a limestone sample for a drainage experiment to reveal the wetting phase distribution changes corresponding to the saturation changes. This study indicates that NMR diffusion measurements and analyses potentially can be used for characterizing pore structure, fluid phase distributions, and permeability in porous systems.

Introduction

The characterization of pore structures of reservoir rocks is of fundamental importance for petroleum exploration and recovery. Although there are a number of conventional methods that attempt to characterize the structures of porous media at a microscopic level, none are without serious limitations and objections. For example, mercury porosimetry is largely insensitive to pore sizes, providing only a measure of pore throat sizes. Furthermore, the method should only be considered to be semi-quantitative since it relies on the bundle-of-tubes model for interpretation of the measurements; that model is known to be a poor representation of media typical of petroleum reservoirs. The use of quantitative stereology with thin sections can provide certain structural information; however, pore connectivity, permeability, and fluid distributions are not observed from such studies.

In recent years, there have been an increasing awareness and interest in the use of NMR diffusion measurements to detect pore structures and other petrophysical properties (Callaghan, 1991; Callaghan, et al.,1990;1991; Mitra and Sen, 1992; Mitra, et al., 1992; Chen, et al., 1992a; Latour, et al., 1993). The approach is based on the fact that the diffusional motion of fluid molecules in the pore spaces of a porous medium is quite different from that in a bulk liquid due to the presence of pore boundaries which restrict the diffusion. The effects of the geometrical restrictions result in measured diffusivities being smaller than those in unrestricted fluids. Using pulsed field-gradient (PFG) NMR techniques, the measured apparent diffusivity can reveal the underlying pore structures. Furthermore, the apparent diffusivities measured using different ranges of diffusion times feature different pore structural information. Thus, experiments can be designed to elucidate a variety of information regarding the microscopic pore structures.

In this work, diffusion measurements were performed in ten sandstone and carbonate samples. These samples were selected to represent a broad range of pore geometrical and permeability differences. A modified version of a stimulated echo sequence with four bipolar gradient pulses (Cotts, et al., 1988) was used in the experiments for the purpose of reducing the effects arising from internal field gradients. The effect of time dependent diffusivity on the echo attenuation was considered and a new expression was derived for the echo attenuation as a function of experimental diffusion

time. Simplified forms were used as expressions for the echo attenuations in analyzing the data. Permeability differences in rocks were related to the diffusivity differences. In addition, fluid phase distribution changes corresponding to different wetting phase saturations for a two-phase drainage process in a Texas Cream limestone were investigated, demonstrating a unique advantage of NMR diffusion measurements for monitoring the fluid phase distributions in multiphase situations.

Background

The usefulness of the NMR diffusion technique for probing pore structures is due to the fact that the observed diffusivity depends on the time over which the diffusional motion is measured. The time dependency is related to the pore size and structure. Thus, by analyzing the diffusion behavior and its time dependency, one can obtain pore structural information.

The diffusion behaviors at short and long diffusion times in porous media have been studied recently (Mitra and Sen, 1992). At short diffusion time region, the diffusivity varies as

$$\frac{D(t)}{D_0} = 1 - \frac{4(D_0 t)^{1/2}}{3d\sqrt{\pi}} \frac{S_p}{V_p} + O(D_0 t), \tag{1}$$

where d is the spatial dimension, D_0 is the bulk liquid diffusivity, and S_p and V_p are the pore surface and volume, respectively. On the other hand, at long diffusion times (Haus and Kehr, 1987),

$$\frac{D(t)}{D_0} = \frac{1}{\alpha} + \frac{\beta_1}{t} - \frac{\beta_2}{t^2}, \tag{2}$$

and the observed diffusivity approaches a constant value: the effective diffusivity D_{eff}.

Echo Attenuation in Porous Media

Stimulated Echo Sequence with Bipolar Gradients

Four-bipolar-gradients stimulated echo sequences, originally developed by Cotts and Coworkers (1988), were used in our measurements. A further modification of the sequence was done by applying a small amplitude crusher gradient during the phase storage time period (Fig. 1) for dephasing the signals from the extra echoes generated by multiple rf pulses.

The echo attenuations using the bipolar gradient stimulated echo sequences are described by

$$\frac{M_{\text{I}}(g_a, t)}{M(0)} = \exp[-\gamma^2 D(b_1 g_a^2 + b_2 g_0^2)] \tag{3}$$

for Sequence I, and

$$\frac{M_{\text{II}}(g_a, t)}{M(0)} = \exp[-\gamma^2 D(b_1 g_a^2 + b_2 g_0^2 + b_3 g_a \cdot g_0)] \tag{4}$$

for Sequence II, where $M(0)$ contains effects due to relaxation. The parameters g_a and g_0 are the applied and internal gradients, respectively. The time coefficients are

$$b_1 = \delta^2 \left(4\Delta + 6\tau - \frac{2\delta}{3}\right), \tag{5}$$

$$b_2 = \frac{4\tau^3}{3}, \tag{6}$$

and

$$b_3 = 4\tau^2\delta. \tag{7}$$

The major advantage of applying bipolar gradient pulses is the cancellation (in the case of Sequence I) or significant reduction (in the case of Sequence II) of the effect due to the internal field gradient. In the latter case, even though the $g_a \cdot g_0$ term is not completely eliminated, the coefficient $b_3 = 4\tau^2\delta$ is not diffusion time Δ dependent, which is different from the corresponding term in the conventional stimulated echo sequence (Tanner, 1970). Since the internal field gradient effect for fluids in porous media can be large due to the inhomogeneities in chemical composition and structure of the porous systems, sequences which can eliminate or reduce such effects are desired. A second advantage of using the bipolar gradient sequence is the 180° rf pulses act similarly to those in the CPMG sequence, thus the effects of T_2 decay during the time period 2τ are greatly reduced.

At any given observation time, if the observed echo attenuation can be regarded as due to a single diffusional process, a single diffusivity is expected. In this case, the term due to g_0^2 is canceled if the ratio of echo amplitudes taken with $g_a = 0$ and with a finite g_a is formed. For Sequence I,

$$\ln R_{\mathrm{I}} = \ln\left[\frac{M_{\mathrm{I}}(g_a,t)}{M(0,t)}\right] = -\gamma^2 D(b_1 g_a^2), \tag{8}$$

and for Sequence II,

$$\ln R_{\mathrm{II}} = \ln\left[\frac{M_{\mathrm{II}}(g_a,t)}{M(0,t)}\right] = -\gamma^2 D(b_1 g_a^2 + b_3 g_a \cdot g_0). \tag{9}$$

Effect of Restrictions: Short Diffusion Times

The expressions in the previous section were originally derived assuming a uniform system without geometrical restrictions. For geometrically restricted systems, such as fluids in porous media, several modifications should be considered.

The quadratic dependence of gradients, shown in Eqs. (8-9) for free diffusion, is a result of a Gaussian distribution of displacements (Mitra and Sen, 1992). Strictly speaking, this postulate is not valid for restricted diffusion. Mitra and Sen (1992) recently used a cumulant expansion approach, and they obtained

$$\ln\left[\frac{M(\mathbf{q},\Delta)}{M(0,\Delta)}\right] = \sum_{n=1}^{\infty} \frac{< \{i\mathbf{q}\cdot[\mathbf{r}(0)-\mathbf{r}(\Delta)]\}^{2n} >}{(2n)!} \tag{10}$$

where $\mathbf{q} = \gamma \mathbf{g}\delta$. The free diffusion case corresponds to $n = 1$ with all the higher order terms vanishing. For porous systems, the higher order terms are not eliminated. Thus, the echo attenuation will depend not only on $\mathbf{q}^2$ terms, but also on $\mathbf{q}^4$, etc. However, for smaller gradients (thus a smaller $\mathbf{q}$) and for short diffusion time, the contributions from higher order terms are not significant. Thoughout this paper, the quadratic term approximation is used, although the effect of higher order terms will be discussed in several places.

Even if only the $n = 1$ term is considered, the echo decay expressions for porous systems are different from those shown in the previous section due to the time dependent diffusivity. Starting from Torry's expression for the Bloch equation with diffusion terms with all assumptions used in Cotts's reference holding, we see that the echo attenuations are represented by

$$\frac{M(g_a,t)}{M(0,t)} = \exp\left\{-\gamma^2 \int_0^t D(t')\left(\int_0^{t'} g(t'')dt''\right)^2 dt'\right\}, \tag{11}$$

where $g(t)$ is the effective gradient, which includes both applied and internal gradients. This differs from the free diffusion cases in that the diffusivity should remain inside the integral. This expression can be approximated as

$$\frac{M(g_a,t)}{M(0,t)} = \exp\left\{-\gamma^2 D(t)\int_0^t \left(\int_0^{t'} g(t'')dt''\right)^2 dt'\right\} \tag{12}$$

for cases of short applied gradients, that is, when the condition $\Delta \gg \delta, \tau$ holds, as has been discussed by Latour et al. (1993) for a case using a somewhat different sequence. Using Sequence I, this approximation yields

$$\frac{M(g_a,t)}{M(0)} = \exp[-\gamma^2 D(t)(b_1 g_a^2 + b_2 g_0^2)], \tag{13}$$

which is similar to Eq. (4) except that D is replaced by $D(t)$.

The integral of Eq. (11) can be evaluated explicitly for the rectangular shape of applied gradients and for the diffusion expression in the form of Eq. (1). For Sequence I in Fig. 1, the diffusion contributions for echo attenuation can be expressed as the combination of two terms, $\ln R_{\rm I} = \ln R_0 + \ln R_r$. The first term is the same as for free diffusion

$$R_0 = \exp\left\{-\gamma^2 \int_0^t D_0 \left(\int_0^{t'} g(t'')dt''\right)^2 dt'\right\}, \tag{14}$$

which will result in Eq. (8). The second term is the modification term due to the restriction effect

$$R_r = \exp\left\{\gamma^2 \int_0^t D_0 \frac{4\sqrt{D_0 t'}S_p}{9\sqrt{\pi}V_p}\left(\int_0^{t'} g(t'')dt''\right)^2 dt'\right\}. \tag{15}$$

The calculation is straightforward, but tedious, and the result is

$$\begin{aligned}\ln R_r \;=\; & D_0\gamma^2 g^2 \frac{4\sqrt{D_0}S_p}{9\sqrt{\pi}V_p}\{\frac{8}{15}\delta[c_1^{2.5} - c_2^{2.5} - 2c_3^{2.5} + c_5^{2.5} - 2c_6^{2.5} - c_7^{2.5}] \\ & + \frac{16}{105}[c_2^{3.5} + c_3^{3.5} - c_4^{3.5} - c_1^{3.5} + c_5^{3.5} - c_6^{3.5} - c_7^{3.5} + c_8^{3.5}]\},\end{aligned} \tag{16}$$

where $c_1 = \delta_1 + \tau$, $c_2 = \delta_1 + \delta$, $c_3 = \delta_1 + \delta + \tau$, $c_4 = \delta_1$, $c_5 = \Delta + 2\tau + \delta_1 + \delta$, $c_6 = \Delta + 2\tau + \delta_1$, $c_7 = \Delta + 3\tau + \delta_1$, and $c_8 = \Delta + 3\tau + \delta_1 + \delta$. All these coefficients are determined from the experimental time parameters.

Effect of Restrictions: Long Diffusion Times

According to Eq. (2), at long observation times, the diffusivity approaches a constant. Thus the long-time scale diffusion experiments give an echo attenuation which depends on boundaries (pore structure) but is independent of the motional parameter (diffusivity) (Callaghan, 1991). Direct calculation using regular geometrical pore boundaries, and more recently, using an average propagator (Callaghan, 1991) reached the same solution for the echo attenuations for the long diffusion time limit in the absence of the higher order terms for **q**. Considering only the quadrtic term, and with a Gaussian distribution of pore sizes, the echo attenuation can be expressed as

$$\ln R_{\Delta\to\infty} = -\frac{\alpha^2 a_0^2}{1+\alpha^2\sigma^2} - \frac{1}{2}\ln(1+\alpha^2\sigma^2), \tag{17}$$

where a_0 = mean and σ^2 = variance of characteristic pore sizes, and

$$\alpha^2 = (2\pi q a)^2/5. \tag{18}$$

Note that in the above expression, diffusivity does not appear explicitly. It is actually represented by the pore size a. The fact that the effective diffusivity is time independent allows one to use the pore size to represent the diffusivity.

The price paid for the approximations used for obtaining the above expression and the omission of the higher power terms of Eq. (10) is the loss of information about the detailed pore geometry. For example, spherical and cubic pores will yield the same expression shown above, except for a scaling factor in the definition of pore size a.

Experimental

All experiments were performed on a GE CSI-II imager/spectrometer system operated at 85 MHz. The system is equipped with 20 Gauss/cm gradient capability. A 1.75 inch diameter birdcage rf coil was used in the experiments.

Ten rock samples, including three types of sandstones (Bentheimer, Brown, and Berea) and two types of carbonates (Texas Cream and Dolomite) were studied. In the cases of Berea, five different samples with different permeabilities were used. Most of the experiments were performed at complete water saturation states. A few experiments were performed at various levels of water saturations. The partial saturations were obtained using a lab-developed desaturation unit. The design and function of the desaturation unit has been described elsewhere (Chen, et al., 1993a). The uniformity of saturations were checked with NMR profile imaging experiments (Chen, et al., 1992b).

Results and Discussion

Demonstration of the Elimination of g_0 Effects

First we demonstrate that the internal gradient effects are effectively eliminated by using the four-bipolar-gradients stimulated echo sequences. Figures 2a and b shows the echo attenuations as a function of gradient strength g_a^2 measured at Δ = 600 ms using both Sequences I and II for water saturated Bentheimer sandstone and Brown sandstone. Bentheimer sandstone is a clean and macroscopically homogeneous sandstone and Brown sandstone is highly heterogeneous in both structure and composition. Thus, the internal gradient strengths for the two samples will be quite different. From Eqs. (8) and (9) we see that the difference in the echo attenuation between the results obtained using the two sequences is proportional to $b_3 = 4\tau^2\delta g_a \cdot g_0$. The fact that the observed differences are within the level of the experimental random noise indicates that the internal gradient effect are negligible when using the bipolar-gradients stimulated echo sequences.

Features of Relationship of Echo Attenuation and Observation Time

Figure 3 shows the echo attenuations as a function of the observation time Δ corresponding to four different samples: Bentheimer and Berea sandstones, Texas Cream limestone and Dolomite. Measurements were performed at complete water saturated states using Sequence I. These rocks have different characteristic pore sizes and the permeabilities differ substantially. The echo magnitudes ($M(0,\Delta)$) corresponding to $g_a = 0$, and $M(g_a,\Delta)$ corresponding to g_a = 19 Gauss/cm, were

measured separately and different preamplification gains were used in the two sets of experiments in order to take advantage of the best S/N. The data in Fig. 3 are the ratio of the two sets with a scaling constant determined experimentally. Different decay rates among these samples were observed. We see that the echo attenuation is strongest in Bentheimer and weakest in dolomite, corresponding to a larger effective diffusivity in Bentheimer and smaller one in dolomite. The differences can be qualitatively explained by the structure and pore size differences of the samples, as fluids in larger pores will experience less restrictions, and in smaller pores more restrictions. The observed difference is consistent with the thin section analysis which shows that Bentheimer has the largest characteristic pores and both the two carbonates contains a certain amount of secondary pores.

Measurements were also performed (Fig. 4) using samples which are of the same rock type, but which have different permeabilities. The permeability values reported by the sample providers are listed in Table 1. There are three different permeability values for the five Berea sandstone samples. The data for the two samples which have a permeability of 100 mD are close together, as are the data for the two samples with a permeability of 300 mD. Generally, the data appear monotonic with increasing permeability, which is consistent with a decrease in diffusional restrictions. This indicates that the echo attenuation can be used as a probe of permeability.

Possibilities of Permeability Evaluation with Diffusion Data

Katz and Thompson (1985) developed a model for estimating absolute permeability in sandstones by relating the permeability K with the pore structure

$$K \propto l_c^2/F, \tag{19}$$

where l_c is the characteristic pore length. With this model, the problem of comparing permeability of different rocks is to find the appropriate estimates for the quantities l_c and F.

One possible approach (Chen, et al., 1993b) is to use the volume-to-surface ratio to represent the characteristic pore length, $l_c = V_p/S_p$, and the porosity to represent the formation factor, $F = \phi^{-m}$, where m is a constant. Recall from Eq. (1) that the quantity V_p/S_p can be obtained from the diffusivity measurements, and thus the diffusivity evaluation can be used to determine the permeabilities.

This approach has the advantage of being easily extended to find relative permeabilities. Using the Archie's empirical relationship (Collins, 1990)

$$\frac{\sigma_{S_w=1}}{\sigma_{S_w}} = S_w^{-n} \tag{20}$$

the relative permeability of the wetting phase can be obtained from the measurements of diffusivities at complete saturation and at a series of partial saturations

$$k_w = \frac{K_w}{K} = \left[\frac{1 - D_{S_w=1}/D_0}{1 - D_{S_w}/D_0}\right]. \tag{21}$$

In this article, only the absolute permeabilities will be discussed.

A quick method for comparing rocks with different permeabilities is described as follows. Recall from Eq. (1) that the diffusivity at $t = 0$ (experimentally, this approximately corresponds to $\Delta = 0$) equals D_0. The time dependent term becomes important when diffusion time is increased; consequently, the echo decay rate decreases with Δ. As Δ increases further, the approximate expression (Eq. (1)) will be generally less valid. For convenience, we can define a quantity, Δ_k,

$$(D_0\Delta_k)^{1/2}\frac{S_p}{V_p} \sim 1. \tag{22}$$

The physical meaning for Δ_k can also be understood by considering that below Δ_k, only a portion of the total molecules within the characteristic pore size V_p/S_p is restricted. Examining Eq. (1) we see that Δ_k can be regarded as a characteristic quantity corresponding to the time below which the linear dependence of D/D_0 vs. $\sqrt{\Delta}$ may be observed.

With the definition specified in Eq. (22) the value of Δ_k can not be determined rigorously. Experimentally, we define the quantity such that the echo decay value at Δ_k is twice that for the time-dependent echo attenuation at $\Delta_k \to \infty$:

$$\ln R_{\rm I}(g_a, \Delta_k) = 2 \ln R_{\rm I}(g_a, \infty). \tag{23}$$

From Eq. (22) we see that

$$(V_p/S_p)^2 \propto \Delta_k, \tag{24}$$

and using Eq. (19) the permeability of the rock depends on Δ_k and F as

$$K \propto \Delta_k/F. \tag{25}$$

Our primary interest is to use the quantity to characterize the permeability differences. For that purpose, we evaluated the permeability ratio

$$\frac{K_{\rm sample1}}{K_{\rm sample2}} = \frac{\Delta_k \phi^{-2}_{\rm sample1}}{\Delta_k \phi^{-2}_{\rm sample2}} \tag{26}$$

with the Bentheimer and Berea data shown in Fig. 3. The values of Δ_k were approximately 320 ms and 130 ms for Bentheimer and Berea, respectively. The porosity values, obtained gravimetrically, are 24.0% and 21.4% for the two rocks. Using these values and Eq. (26), we find $K_{\rm Ben}/K_{\rm Berea}$=2.0. This result agrees reasonably well with that calculated using the permeability values obtained from conventional techniques by the sample providers: 1200/500=2.4.

More comparisons were performed using the Berea data shown in Fig. 4. The results are shown in Table 1. Again, the calculated results with diffusion data show reasonable agreements with those from the permeability values given by the sample providers. We emphasize that even though this method may not be rigorously quantitative, it provides a relatively simple comparison of rock permeabilities over a relatively large scale.

Short Diffusion Time Behavior

From the Δ dependence of echo attenuation, one can evaluate the diffusivity dependence as a function of time. In Fig. 5 we plot a set of the $D(t)/D_0$ curves calculated using the data shown in Fig. 4 for the Berea sandstones and with Eq. (13). Several data corresponding to the shortest Δ's were omitted since the conditions for the validity of the approximation (Eq. (13)) are not satisfied in the very short time region, as described in the section *Echo Attenuation in Porous Media.* In the above analysis, the time dependent apparent diffusivities were evaluated using experimental results acquired only at two gradient values (g_a = 0 and g_a = 19 Gauss/cm) for every observation time. The validity of this approach requires that a linear dependence between $\ln R_{\rm I}$ and g_a^2 be observed. However, this condition is generally only observed during relatively short diffusion times, and may begin to be violeted at Δ = 50 ms, even for rocks with relatively larger pores, such as for Berea 1 (see Fig. 6). Thus rigorous models need to be developed for the recovery of $D(t)$ from those individual curves to improve the accuracy in estimating permeabilities. Even in this case, the experimental time could be very long since large numbers of data curves such as those shown

in Fig. 6 need to be acquired. For estimation of sandstones with large differences in permeabilities, the method we described earlier can provide quick results.

We do not try to compare limestone permeability with those of sandstones. Most limestones contain distinctly different groups of characteristic pore sizes–typically primary and secondary pores. While the porosity in these systems is largely affected by the primary pores, the permeability is largerly affected by the secondary pores. These effects may be included by using the effective diffusivity to describe the formation factor F in Eq. (25). Detailed discussion of this subject will not be included here.

Saturation-Dependent Fluid Distributions

One application of the diffusion measurements corresponding to long diffusion times is the evaluation of fluid phase distributions at different saturations. For a drainage process involving gas (N_2)-liquid (water) phases, it is expected that the wetting phase saturates smaller sized pores at lower saturations due to the capillary effects. Such observations can be confimred by analyzing the diffusion data obtained at different saturations. For this purpose, the long observation time ($\Delta = 600$ ms) diffusion measurements were performed at several saturation levels. The Gaussian distribution model (Eq. (17)) was used for representation of pore sizes. At complete water saturation, the distribution reflects the pore size distribution of the entire sample while at partial saturations, the pore size distribution obtained corresponds to the water phase occupancy (i.e., the wetting fluid phase distribution). Figure 7 plots the fluid phase distributions obtained using the above analysis in a Texas Cream limestone sample. It is observed that the distribution curve shifts to the left as saturation is lowered, consistent with the drainage process. It is also noted that the mean value of the distribution of the fully saturated case, $a_0 \approx 60\mu$m, agrees with the mean value of the pore sizes obtained by thin-section analysis; the latter showed that $<a> \approx 60 - 100\mu$m. The advantage of using the NMR technique is obvious: it provides not only the pore size distribution at complete saturations, but also the fluid phase distributions at any saturation levels. It is also more appropriate for quantitative evaluation, compared to thin-section photography.

The Gaussian distribution model provides a reasonable fit to the echo attenuation, as can be seen in Fig 8. Other models, including the single-sized spherical pore model and single-sized cubic pore model (Callaghan, 1991), have also been tested but failed to provide satisfactory fits. The outcome is expected considering the heterogeneous nature of natural porous rocks. However, the curvilinear behavior of $\ln R_I$ vs. g_a^2 may also be due to the contribution of higher terms, g_a^{2n}, which have been omitted in Eq. (17).

Summary

NMR diffusion measurements in a number of rocks samples with different pore structures revealed that the rock permeabilities can be detected by analyzing the differences in restricted diffusion effects.

The short diffusion time behavior of echo attenuation for the cases of time-dependent diffusivity can be expressed as the product of the attenuation due to free diffusion (diffusion-time-independent) and the term corresponding to the restricted diffusion effect (diffusion-time-depednet). The exact expression is derived.

The fluid phase distributions corresponding to different saturations for a two-phase system can be obtained by analyzing the echo attenuation corresponding to the long diffusion time. The mean pore size obtained from diffusion measurements and from thin-section analysis are in a good agreement.

Acknowledgment

This research was supported in part by DOE Grant #DE-FG07-89BC14446 and by a University-Industry Cooperative Research Program at Texas A&M University.

Nomenclature

a	=	pore size
a_0	=	mean pore size
d	=	spatial dimension
D	=	diffisivity in porous media
D_{eff}	=	effective diffisivity at long diffusion time
D_0	=	bulk fluid diffisivity
F	=	formation factor
g	=	effective gradient
g_0	=	internal gradient
g_a	=	applied gradient
K	=	absolute permeability
k_w	=	relative permeability
l_c	=	characteristic pore length
$M(g_a, t)$	=	intensity of magnetization
$M(0, t)$	=	intensity of magnetization at $g_a = 0$
q	=	wave factor $= \gamma \delta g$
R	=	ratio of intensities
S_p	=	pore surface
S_w	=	fluid saturation
V_p	=	pore volume

Greek Letters

γ	=	proton gyromagnetic ratio
δ	=	gradient length
σ^2	=	variance of characteristic pore size
σ_{S_w}	=	conductivity of porous media at saturation S_w
ϕ	=	porosity
τ	=	pulse sequence time parameter
Δ	=	experimental diffusion time

References

Banava, J., and Schwartz, L. M., in *Molecular Dynamics in Restricted Geometries*, Ch. 10, edited by Klafter, J. and Drake J. M., (John Wiley & Sons, New York, 1989).
Callaghan, P. T., *Principles of Nuclear Magnetic Resonance Microscopy*, (Clarendon Press, Oxford, 1991).
Callaghan, P. T., MacGowan, D., Packer, K. J., and Zelaya, F. O., *Nature* (London) **351**, 443 (1991); *J. Mag. Reson.* **90**, 177 (1990).
Chen, S. Liaw, H.-K., and Watson, A. T., *J. Appl. Phys.*, in press, (Aug. 1, 1993a).
Chen, S. Liaw, H.-K., and Watson, A. T., *Mag. Reson. Imag.*, in press (1993b).
Chen, S., Miao, P., and Watson, A. T., *SPE* #24812, 477-489 (1992a).
Chen, S., Kim, K. Qin, F., and Watson, A. T., *Mag. Reson. Imag.* **10**, 815 (1992b).
Collins, R. E., *Flow of Fluids Through Porous Materials*, 2nd reprint, (Research & Engineering Consulatants, Inc., Englewood, CO, 1990).
Cotts, R. M., Hoch, M. J. R., Sun, T., and Markert, J. T., *J. Mag. Reson.* **83**, 252-266 (1989).
Halperin, W. P., D'Orazio, F., Bhattacharja, S., and Tarczon, J. C., in *Molecular Dynamics in Restricted Geometries*, Ch. 11, edited by Klafter, J. and Drake J. M., (John Wiley & Sons, New York, 1989).
Haus, J. W. and Kehr, K. W., *Phys. Rep.* **150**, 263 (1987).
Katz, A. J. and Thompson, A. H.,*Phys. Rev. B* **34**, 8179 (1985).
Latour, L. L., et al., *J. Mag. Reson. Ser. A* **101**, 342-346 (1993).
Mitra, P. P., and Sen, P. N., *Phys. Rev. B* **45**, 143-156 (1992).
Mitra, P. P., Sen, P. N., Schwartz, L. M., and Doussal, P. Le, *Phys. Rev. Lett.* **68**, 3555 (1992).
Roberts J. N., and Schwartz, L. M., *Phys. Rev. B***31**, 5990 (1985).
Tanner, J. E., *J. Chem. Phys.* **52**, 2532 (1970).

Table 1. Physical parameters of Berea samples

parameter	Berea 1	Berea 2	Berea 3	Berea 4	Berea 5
ϕ (%)	21.4	19.3	21.2	18.4	17.9
Δ_k (ms)	130	62	66	22	20
K^* (mD)	500	300	300	100	100
K^*/K^*_{Bereal}	1	1.7	1.7	5	5
K/K_{Bereal}	1	1.8	1.9	4.4	4.6

Explanations:
1. K^* values were given by the sample providers and K values were calculated using our diffusion data.
2. Berea samples 1, 3, and 5 were from one provider, samples 2 and 4 from a different provider.

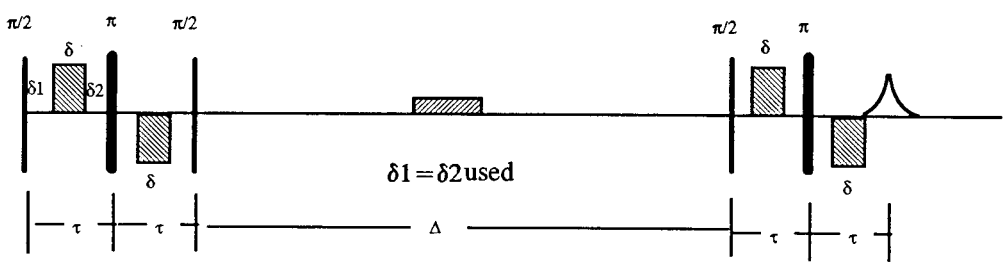

(a)

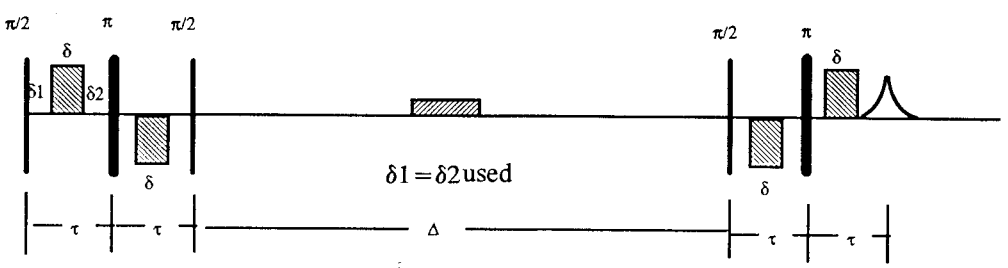

(b)

Fig. 1. (a) Bipolar-gradients stimulated echo sequence I. (b) Bipolar-gradients stimulated echo sequence II.

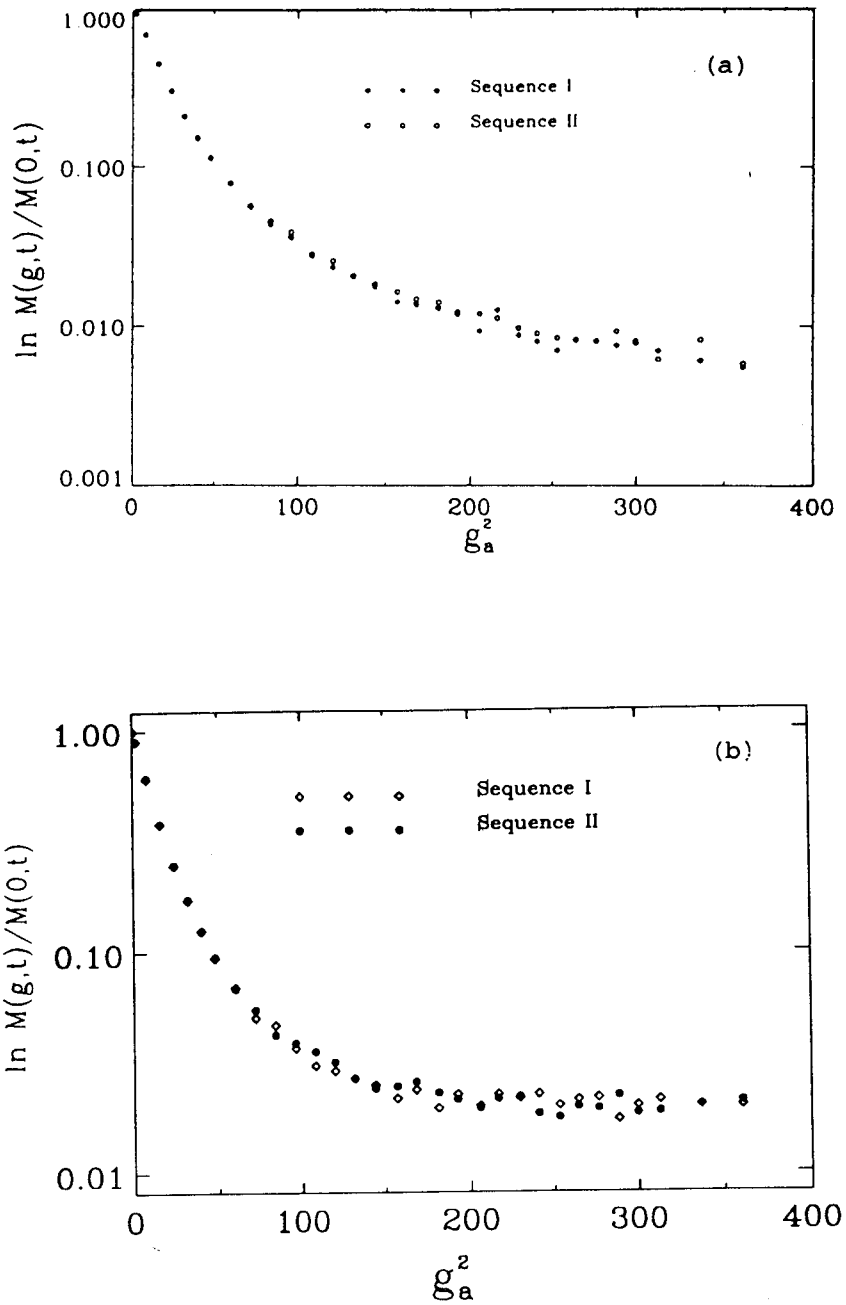

Fig. 2. Comparison of the echo attenuations measured by Sequences I and II for (a) Bentheimer and (b) Brown sandstones.

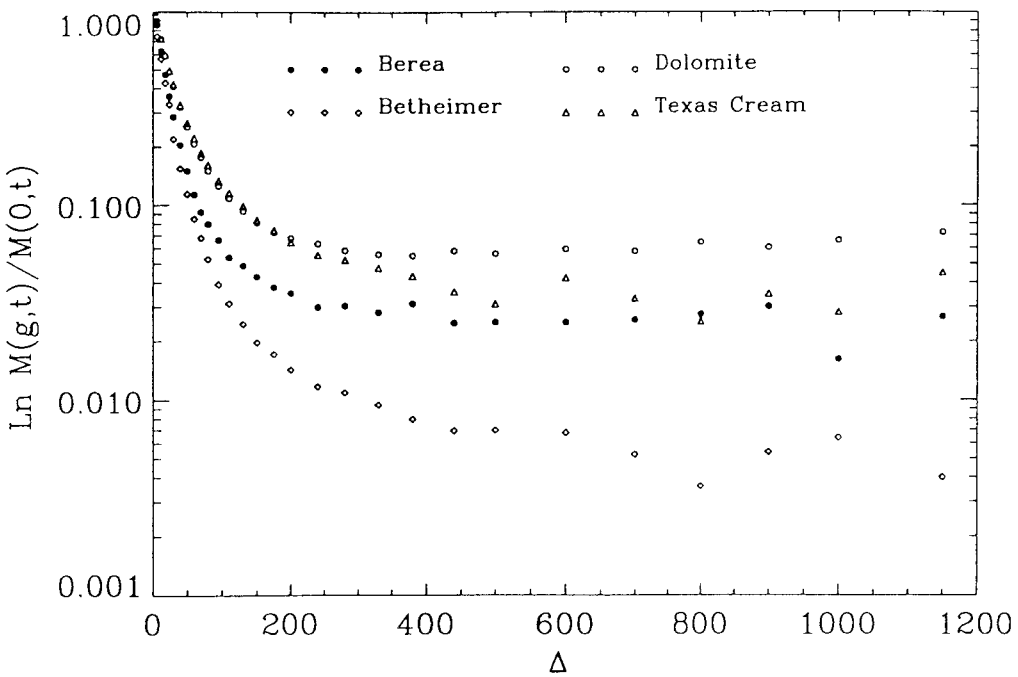

Fig. 3. Measured diffusion time dependent echo attenuations for four samples.

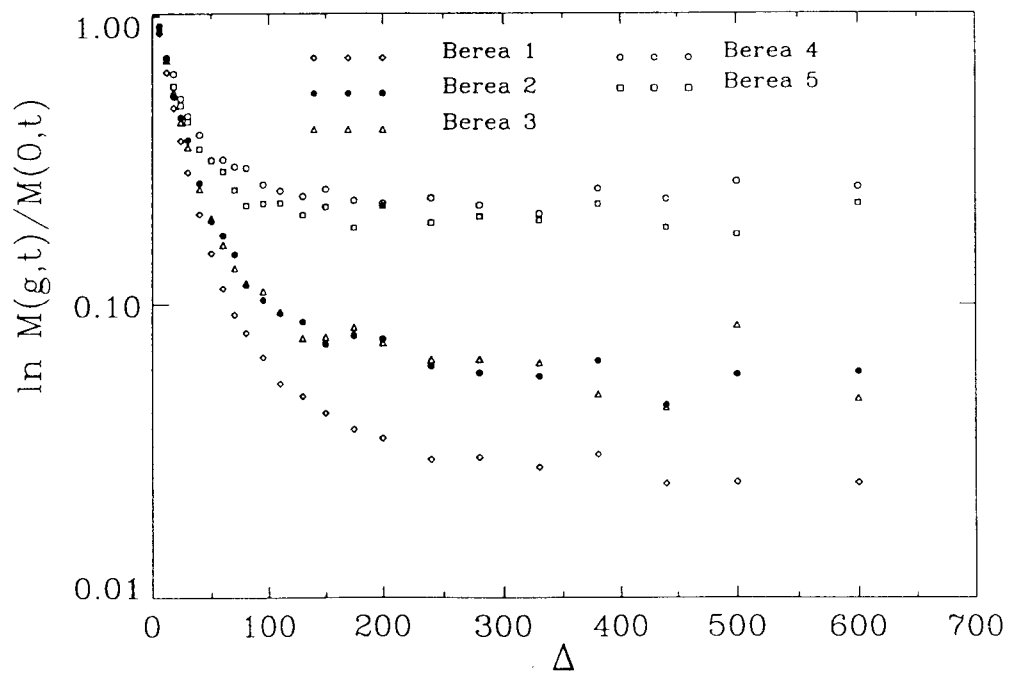

Fig. 4. Measured diffusion time dependent echo attenuations for five Berea sandstones having different permeabilities.

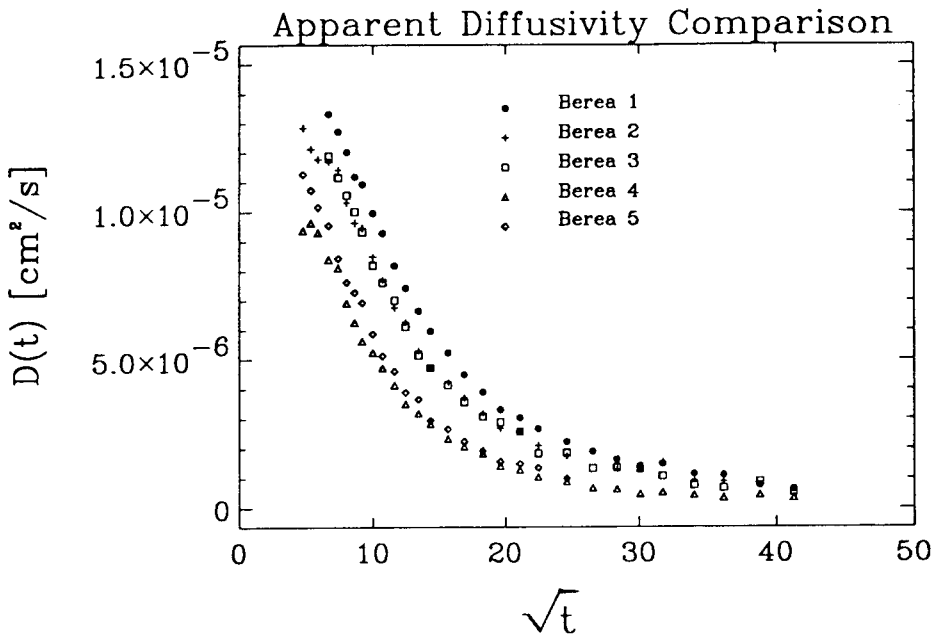

Fig. 5. Apparent diffusivity with its observation time dependency for the five Berea sandstones. The trends are consistent with the permeability differences

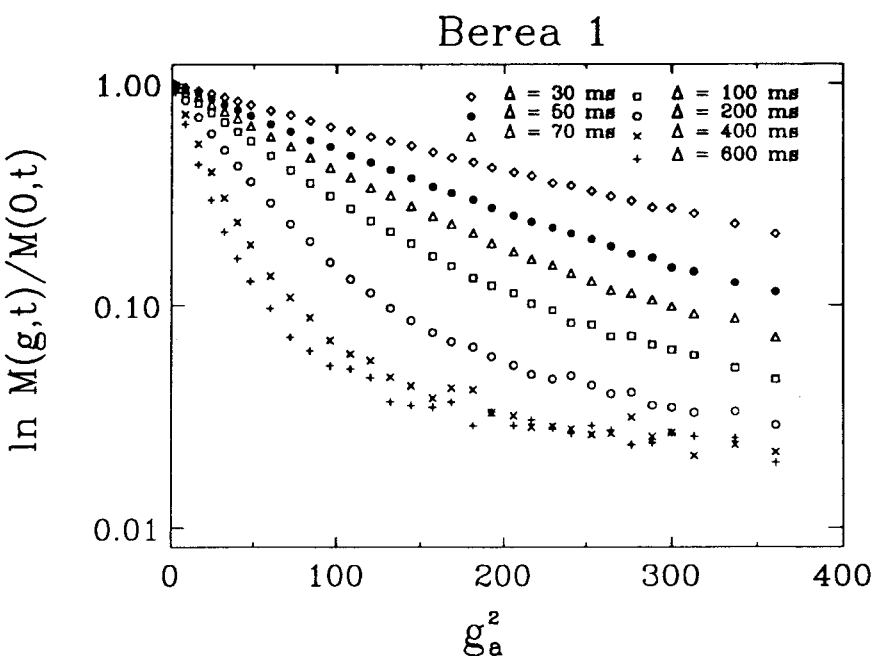

Fig. 6. The gradient strength dependency of the echo attenuations for Berea 1 at various observation times. Linear dependence was observed for short observation times only.

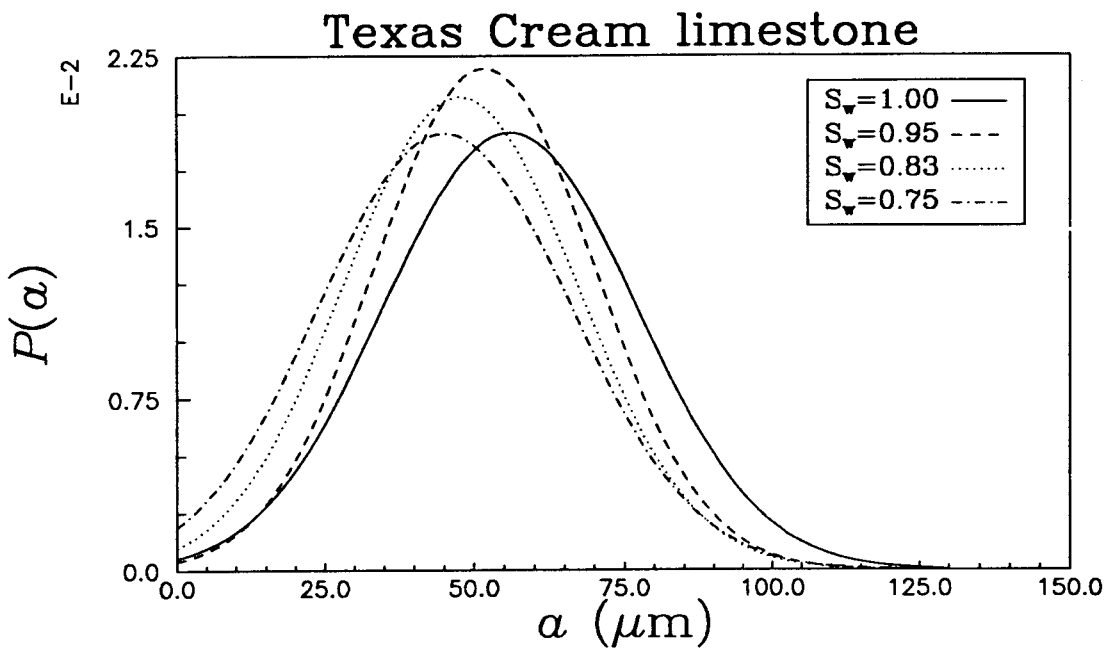

Fig. 7. Wetting phase distributions obtained at various saturation levels for Texas Cream limestone. The figure indicates the distribution changes with saturation, which is consistent with a drainage process.

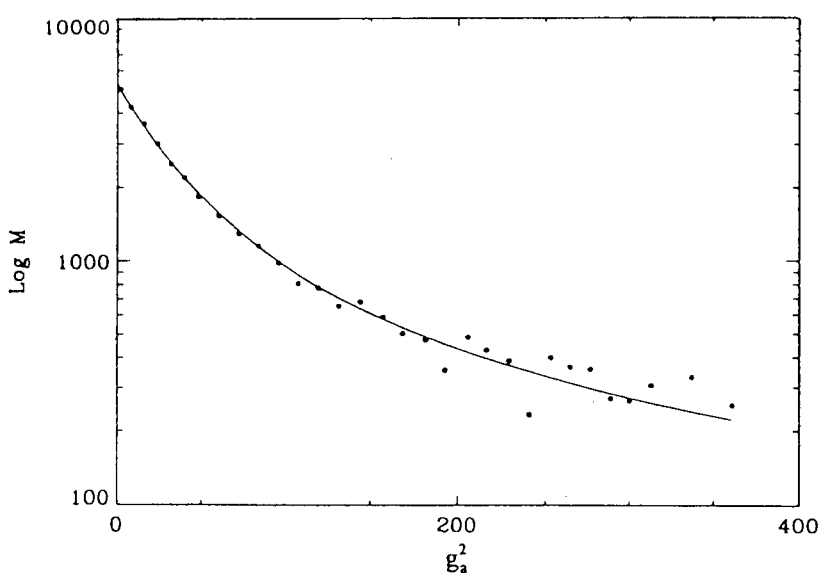

Fig. 8. The fitting quality using a model with Gaussian distribution of pore sizes.